Biological Journal of the Linnean Society, 2017, **121**, 923–935. With 6 figures.

Comparison of cranial performance between mainland and two island subspecies of the Arctic fox *Vulpes lagopus* (Carnivora: Canidae) during simulated biting

OLGA NANOVA[1*], MIGUEL PRÔA[2,3], LAURA C. FITTON[4], ANDREJ EVTEEV[5] and PAUL O'HIGGINS[4]

[1]*Zoological Museum of Lomonosov Moscow State University, Bol'shaya Nikitskaya, 6, Moscow 125009, Russia*
[2]*Centro de Investigação em Antropologia e Saúde, Universidade de Coimbra, Departamento de Ciências da Vida, Apartado 3046, 3001-401 Coimbra, Portugal*
[3]*Centre for Anatomical and Human Sciences, The Hull York Medical School, University of York, Heslington, York YO10 5DD, UK*
[4]*Department of Archaeology and the Centre for Anatomical and Human Sciences, The Hull York Medical School, University of York, Heslington, York YO10 5DD, UK*
[5]*Anuchin Research Institute and Museum of Anthropology of Lomonosov Moscow State University, Mokhovaya, 11, Moscow 125009, Russia*

Received 13 January 2017; revised 20 February 2017; accepted for publication 20 February 2017

Island subspecies of the Arctic fox *Vulpes lagopus* differ morphologically from the mainland subspecies. In particular, differences in cranial form may reflect varied biomechanical adaptations associated with hunting and feeding behaviours. We tested the hypothesis that the observed cranial differences between two island foxes (living on two North Pacific islands) and those living on the mainland have no impact on biomechanical performance during simulated biting. 3D cranial models of three Arctic fox subspecies were compared based on biomechanical parameters (e.g. local strain and large-scale deformation). Finite elements (FE) analyses were used to simulate equivalent biting loads, and geometric morphometrics was used to compare the modes of deformation among the models. The results showed differences in local strains and modes of global deformation among the three subspecies; the mainland subspecies was particularly distinct from the island subspecies. The representative cranium of the mainland subspecies experienced higher strain than that of both island subspecies during all bites. However, the findings highlight issues that arise when relating biomechanical performance, measured via FE analyses, to the foods consumed rather than to the mechanical properties of the individual's diet. Additional physical properties data for each prey type are necessary to determine the extent to which the present findings reflect biomechanical adaptations to diet and prey acquisition.

ADDITIONAL KEYWORDS: finite elements analysis – geometric morphometrics – island isolation – Arctic fox.

INTRODUCTION

Isolated island populations undergo rapid phenotypic changes compared to mainland populations of the same species (Mayr, 1967; Gould & Eldredge, 1977; Millien, 2006). This is true for the Arctic fox *Vulpes lagopus* L., 1758, whose island populations undergo rapid phenotypic change. Arctic foxes on the two Commander Islands, Bering and Mednyi (200 km from the west coast of the Kamchatka Peninsula in the Russian Bering Sea; Fig. 1), have been isolated for approximately 10 000 years from mainland Arctic foxes (located on the Chukchi Peninsula in far east continental Russia) (Goltsman, Kruchenkova & Macdonald, 1996; Goltsman *et al.*, 2005; Geffen *et al.*, 2007; Dzhykiya, 2008) by the ice-free waters of the Bering Sea. Genetic data show that the two populations of the Commander Islands not only cluster together, but are also the most genetically different from all other Arctic fox populations (Geffen *et al.*, 2007). The average pairwise differences calculated from mtDNA between island populations and other Arctic fox populations

*Corresponding author. E-mail: nanovaolgag@gmail.com

are 9.06–14.78. The distance between Mednyi and Bering Island foxes is 3.24 (Dzhykiya, 2008).

Food sources available to Arctic foxes living on the Commander Islands differ from those available to the mainland population (Angerbjörn, Tannerfeldt & Erlinge, 1999; Anthony, Barten & Seiser, 2000; Zagrebelnyi, 2000a; Goltsman *et al.*, 2010; Table 1). Rodents such as lemmings (*Lemmus* and *Dicrostonyx*) and voles (*Microtus*, *Clethrionomys*, and *Arvicola*) are generally the main prey of Arctic foxes on the mainland throughout the year (Angerbjörn *et al.*, 1999; Anthony *et al.*, 2000; Eide, Jepsen & Prestrud, 2004). However, rodents are absent on Mednyi Island and, although the Northern red-backed vole was introduced to Bering Island, it plays a minor role in the diet of foxes there (Zagrebelnyi, 2000b). The main summer food sources for foxes on the Commander Islands are seabirds, especially the Northern fulmar (*Fulmarus glacialis*), which forms great rookeries on the islands and can amount to about 90% of the Arctic fox diet (Goltsman *et al.*, 2010). While small rodents are caught relatively easily by Arctic foxes and swallowed whole, large seabirds need to be held strongly until death, and only then can Arctic foxes eat the flesh. The second rich food source available during the summer is the Northern fur seal (*Callorhinus ursinus*): foxes scavenge carcasses and placentas and prey on new-born fur seal pups (Chelnokov, 1970; Naumov *et al.*, 1981). In winter, when preferred prey are scarce, island foxes primarily forage on the carcasses of marine mammals, including sea otters (*Enhydra lutris*) (Zagrebelnyi, 2000a; Goltsman *et al.*, 2010). The skin of pinnipeds is thick and tough, and Arctic foxes usually choose the weakest (softest) parts of the carcass to eat, such as muzzle and anus. But unlike Polar bears (*Ursus maritimus*), which rip open the skin of seals with their claws (Sacco & Van

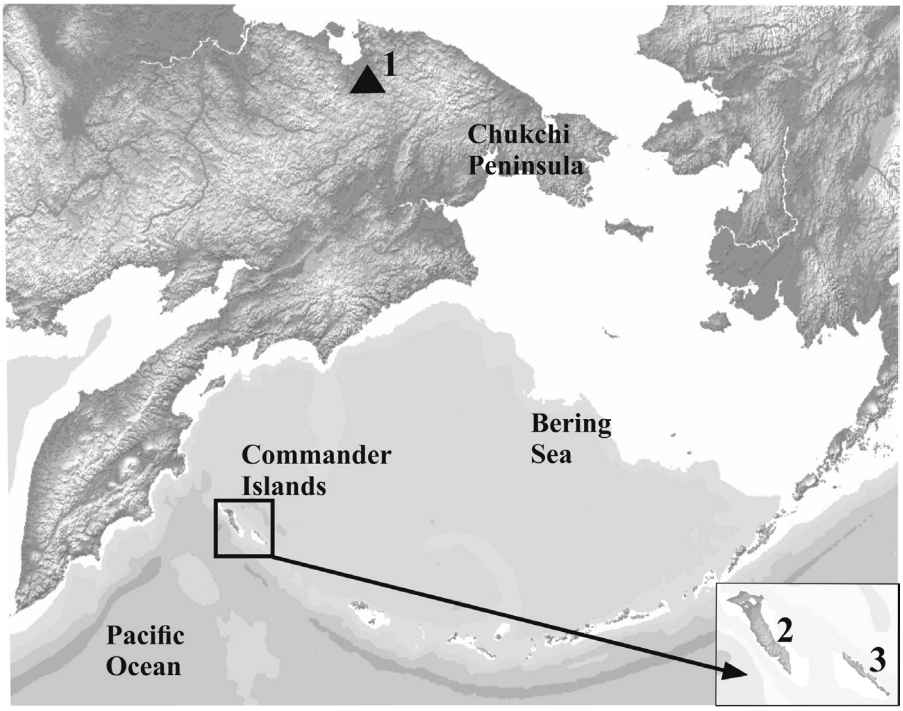

Figure 1. Map of the Bering Sea region, showing the location of the two Commander Islands 200 km off the eastern coast of Kamchatka Peninsula, in the ice-free part of the Bering Sea, and the location where the mainland specimen was collected. Provenance of specimens: 1, Mainland, Chukotka, Chaunsky District; 2, Commander Islands, Bering Island; 3, Commander Islands, Mednyi Island. The copyright-free map was downloaded from http://www.maps-for-free.com/ and modified.

Table 1. Arctic foxes subspecies, their localities and main diet

Subspecies	Locality	Main diet
Vulpes lagopus semenovi	Mednyi Island (Commander Islands)	Large seabirds; marine mammal carcasses
Vulpes lagopus beringensis	Bering Island (Commander Islands)	Large seabirds; marine mammal carcasses
Vulpes lagopus lagopus	Mainland (Chukotka, Chaunsky District)	Small rodents

Valkenburgh, 2004; Christiansen, 2007; Figueirido *et al.*, 2009; Slater *et al.*, 2010; Kupczik & Stynder, 2012), Arctic foxes use primarily their jaws and teeth for cutting prey, which causes a considerable mechanical constrain on the skull morphology.

During times of isolation in unusual conditions, Arctic foxes have undergone sufficient morphological changes that justify their classification as different subspecies (Table 1). Thus, populations living on Mednyi Island have been assigned to *V. lagopus semenovi* (Ognev, 1931), and those living on Bering Island to *V. lagopus beringensis* (Merriam, 1902). Arctic foxes living on the mainland (*V. lagopus lagopus*, L., 1758) migrate extensively and effectively constitute a single mainland subspecies (Dalén *et al.*, 2005).

There are numerous morphological differences between island and mainland Arctic foxes (Tcalkin, 1944; Zagrebelnyi & Puzachenko, 2006; Nanova, 2009, 2010). Previous studies have indicated that the island subspecies have greater body and cranial size than is found on the mainland (Tcalkin, 1944; Goltsman *et al.*, 2005; Zagrebelnyi & Puzachenko, 2006; Nanova, 2009, 2010). Moreover, both island subspecies are significantly heavier than their mainland conspecifics, with average winter body masses of 5.0–7.0 kg for males and 4.5–6.0 kg for females, whereas these values on the mainland are 3.2–4.5 kg for males and 3.0–3.5 kg for females (Goltsman *et al.*, 2005). The cranium differs between island and mainland subspecies not only in size but also in shape, as it is longer and wider at the carnassials and zygomatic arches, with relatively stronger developed crests, in both island subspecies (Nanova, 2009). The morphological differences between island and mainland subspecies arise in part through differences in growth. For instance, island foxes have a longer growth period (up to 2 years) in comparison to mainland foxes that complete growth in 1 year (Zagrebelnyi, 2000b). Age-specific allometric trajectories of the cranium also differ between mainland and island subspecies (Nanova, 2010). Mednyi Island and Bering Island subspecies have slight differences in cranium shape as well (Zagrebelnyi, 2000b; Nanova, 2009), but these differences are much weaker than between islands and mainland. The proportion of rostrum and braincase is the most variable between islands, with Mednyi Island foxes possessing significantly shorter rostrum in comparison to Bering Island foxes (Nanova & Prôa, 2017), and rostrum length is related to bite force (e.g. Christiansen & Wroe, 2007; Figueirido et al., 2011). The cranial peculiarities of the island fox subspecies may have arisen as adaptations to specific environmental conditions such that differences in cranial size and shape represent different biomechanical adaptations of mainland and island subspecies crania that impact on performance. For example, a more robust and wider cranium may reduce cranial deformations when handling tough food items (e.g. cutting the skin of fur seal carcasses).

In the present study, we test the null hypothesis that the observed cranial differences between Arctic foxes living on both the Mednyi and Bering Islands and those living on the mainland have no impact on biomechanical performance during simulated biting. If this is falsified, the question arises as to whether the differences in cranial morphology and performance among the subspecies reflect biomechanical adaptations to their distinct hunting and feeding behaviours and/or if they are the consequence of random processes like genetic drift and founder effect.

Cranial models of the three subspecies were compared based on their biomechanical performance (local strains and large-scale deformations). Finite elements (FE) analyses were used to simulate cranial loading during different bite scenarios, and geometric morphometrics were employed to compare overall cranial deformation. We analysed differences at the subspecies level, while previous studies of cranial performance in mammals using FE modelling have compared higher-level taxa (Dumont, Piccirillo & Grosse, 2005; Wroe *et al.*, 2007; Wroe, 2008; Slater, Dumont & Van Valkenburgh, 2009; Slater & Van Valkenburgh, 2009; Cox *et al.*, 2012; Figueirido *et al.*, 2014).

MATERIAL AND METHODS

The dry crania of three adult male Arctic foxes of known provenance (shot in the wild) were accessed from the Zoological Museum of Moscow State University M.V. Lomonosov (Fig. 1):

1. *Vulpes lagopus lagopus*, Mainland (Chukotka, Chaunsky District, Russian Federation), approx. coordinates 68°26′N 171°39′E, collected in 1972, museum number S-97529;
2. *Vulpes lagopus beringensis*, Bering Island (Commander Islands, Russian Federation), approx. coordinates 55°4′N 166°4′E, collected in 1927, museum number S-30378;
3. *Vulpes lagopus semenovi*, Mednyi Island (Commander Islands, Russian Federation), approx. coordinates 55°45′N 167°33′E, collected before 1946, museum number S-12026.

The crania were scanned using a medical X-ray computed tomography (CT) scanner (Picker PG 2000 CT scanner; Moscow State University of Medicine and Dentistry, X-ray department) with a voxel size for each specimen of 0.23 × 0.23 × 0.33 mm. Image segmentation was performed in Avizo (v.7.0.1, Visualization Sciences Group, Burlington, USA) using a combination of automated thresholding and manual segmentation

to accurately identify bone outlines where automated thresholding failed. Each cranium was modelled as a single material volume (including teeth). Based on the findings of previous sensitivity studies (Fitton *et al.*, 2015), simplifications in FE models result in a consistent reduction in the magnitude of deformation (measured e.g. as strain, or terms of global changes in size and shape), but have minimal effect on relative strains among cranial regions (modes of deformation). The resulting volume data for each specimen were downsampled to a voxel size of 0.4 × 0.4 × 0.4 mm. The voxel-based reconstruction was subsequently transformed into an FE mesh, composed of 8-noded cubic elements by direct voxel conversion. This was carried out using VOX-FE v. 2.0, which is an FE analysis voxel-based software tool developed in the Departments of Computer Science and Engineering, and The Hull York Medical School, University of Hull, UK (Fagan *et al.*, 2007; Liu *et al.*, 2012).

Material properties typical of bone were assigned to the elements in VOX-FE, and loads and constraints to simulate biting (see below) were added to each model. Young's modulus (17 GPa) and Poisson's ratio (0.30) values were assigned to the single material (Kupczik *et al.*, 2007). Maximum muscle forces (Table 2) were calculated using the formula: F_{max} = CSA × k, where k is the specific tension constant (37 N/cm^2; Weijs & Hillen, 1985; Fitton, 2007), and CSA the estimated cross-sectional area of the muscle. Since no muscle data are associated with these specimens, muscle cross-sectional areas were estimated using bony proxies. This method has been used by others (Demes & Creel, 1988; Thomason, 1991; Antón, 1999; Christiansen & Adolfssen, 2005; Ellis *et al.*, 2008), and allows cross-sectional area to be estimated from the dry bone. In this study, two main adductor jaw muscles were included, the superficial masseter *musculus masseter* and temporalis *musculus temporalis*. The estimated cross-sectional area for these muscles was estimated following protocol of Thomason, 1991. The 'temporalis' area was bounded by the zygomatic arch and braincase in a posterodorsal view. The masseter area was bounded by the zygomatic arch and basicranium. Estimated cross-sectional areas on both sides of each cranium were calculated and then averaged for the fluctuating asymmetry accounting. The F_{max} was calculated from this averaged value for each muscle was then applied symmetrically to the both sides of FE model to make the loading symmetrical on both left and right sides. Muscle force orientations were estimated by directing the force vectors from the muscle centre of origin to the muscle insertion point on the mandible, with the mandible in occlusion (Fig. 2). However, since we were only concerned with the cranium, the mandible was not included in the FE analysis.

To prevent free body motion, the models were constrained at the temporo-mandibular joint on the ventral side of the zygomatic process of the squamosal along all three axes (on both sides). To simulate unilateral bites, the models were constrained vertically along the left side dental row at seven different positions: (1) the incisors (which included the simultaneous loading of all three left I^1, I^2, and I^3); (2) the left canine (C); (3) left P^1; (4) left P^2; (5) left P^3; (6) the left upper carnassial (P^4); and (7) a molar (M^1). All teeth were constrained in a dorsoventral direction perpendicular to the occlusal plane.

The FE models were solved using the Linux-based custom built solver software *PARA_BMU*, which is a modified iterative solver similar to that reported by van Rietbergen *et al.* (1996), which was developed in the Departments of Engineering and Computer Science, University of Hull, UK (Fagan *et al.*, 2007; Liu *et al.*, 2012). Von Mises' strain contour plots were obtained and visually assessed. For visual comparison among specimens, the strains in each contour plot for each bite simulation were scaled (linearly based on predicted bite; Hooke's law) to represent a bite force of 400 N, which is close to the estimated natural carnassial bite force of this species (Christiansen & Adolfssen, 2005).

Geometric morphometric methods were employed to compare the modes of global (large-scale) deformation of the models (O'Higgins *et al.*, 2011; Fitton *et al.*, 2012; O'Higgins & Milne, 2013; Fitton *et al.*, 2015). The coordinates of landmarks from the resulting deformed models were subjected to a Procrustes size-and-shape analysis (O'Higgins & Milne, 2013; Fitton *et al.*, 2015), performed using the EVAN toolkit (http://www.evan-society.org). In this analysis, 50 three-dimensional

Table 2. Maximum estimated cross-sectional area (CSA) and muscle forces

Model	*musculus masseter*		*musculus temporalis*	
	CSA (cm^2)	Muscle force (N)	CSA (cm^2)	Muscle force (N)
Mednyi Island	9.24	342	10.24	379
Bering Island	8.89	329	10.92	404
Mainland	8.00	296	8.68	321

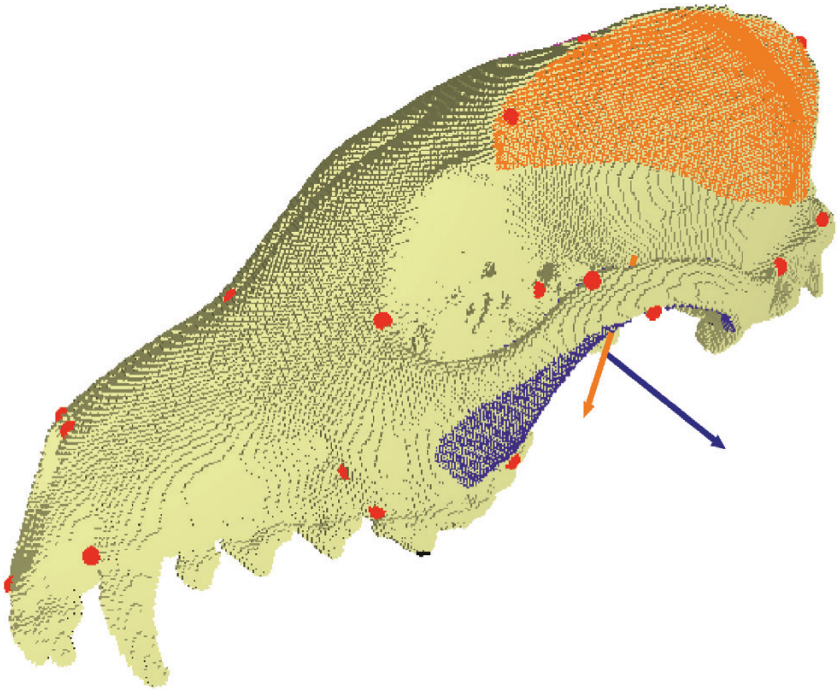

Figure 2. Finite elements (FE) model boundary conditions for the Bering Island fox. Muscle forces represent the major muscles of mastication: purple = masseter; orange = temporalis. Arrows represent muscle force direction for the respective muscle. The glenoid fossae are constrained in all directions and the bite points are constrained in the vertical axis. A P^4 bite is illustrated (a black area shows the constraint at the tip of the tooth). The sampling points (corresponding to the 50 landmarks used for the shape analysis) are shown as red landmarks. Strain magnitudes and three-dimensional coordinates are extracted at these points for comparisons of local and large-scale deformations.

landmarks (Fig. 3 and Table 3) were recorded from each loaded cranium and from the original unloaded models. The large-scale cranial deformations are very small compared to the differences in size and shape among them. Therefore, it is necessary to focus the analysis on the deformations rather than on the differences between specimens. To achieve this, the landmark coordinates of each load case and unloaded model were subjected to generalized Procrustes analyses. The differences between the registered landmark coordinates in each loaded and unloaded cranium were then added to the mean of the unloaded foxes from the GPA, and the resulting configurations were rescaled by multiplying each coordinate by the ratio of centroid sizes between loaded and unloaded models. Size-and-shape coordinates were then calculated by translating and rotating (but not scaling) these configurations to minimize the sum of the squared differences between them. The resulting configurations were then subjected to size-and-shape principal component analyses (PCA) to compare modes of global deformation among crania. The distances between biting simulations examined via PCA did not directly relate to engineering quantities such as strain energy (see Bookstein, 2013; O'Higgins & Milne, 2013). However, they represented differences in the changes in size and shape when loaded.

RESULTS

Strain contour plots are presented in Figure 4. The regions of the cranium that experienced high strain during all bites were the rostrum, the orbit, and the zygomatic arch. In all three models, strains in the rostrum, frontal regions, and zygomatic arch were maximal during the canine bite. During incisors bite, strains in the rostrum and frontal region were also high. The zygomatic arch showed the greatest surface strain relative to the rest of the cranium during P^1, P^2, and P^3 bites. During P^4 biting (carnassial tooth), large strains were present over the maxilla, the medial wall of the orbit, and the temporal bone. This contrasts with P^1–P^3 biting simulations where the largest strain magnitudes were found over the maxilla and frontal bone. During M^1 biting, strains were low over the rostrum and high over the medial wall of the orbit. The medial wall of the orbit and maxillary root of the zygomatic arch were highly strained during P^4 and M^1 bites in all the three models.

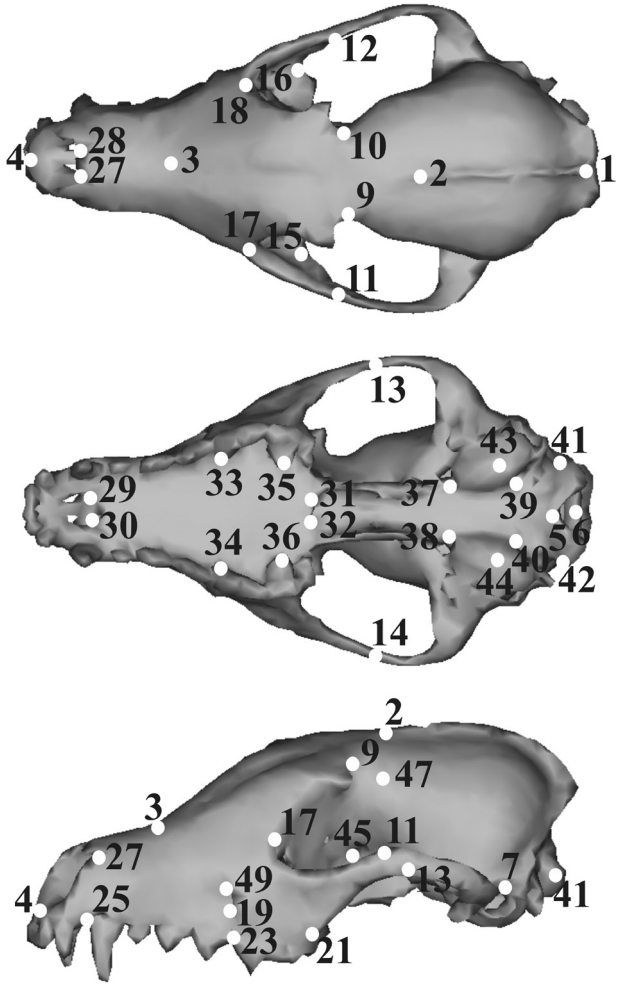

Figure 3. The 50 landmarks used in the geometric morphometric analyses to assess large-scale deformations of the cranium are shown as white dots on the cranium (see Table 3 for landmark description).

Strain comparisons among models (Fig. 4, and Supporting Information, Tables S1–S7) show that the representative cranium of the mainland subspecies experienced higher strains than that of either island subspecies during all bites. The greatest differences between mainland and island subspecies were observed during premolar bites, including the carnassial bite, with strains generally lower in the island subspecies, particularly in the zygomatic arch. In the orbital region, during P^4 and M^1 bites, strains were also lower in the island foxes. Strain contours were rather similar for both Bering Island and Mednyi Island foxes, and regions of high strain were smaller than those observed in the mainland fox. Nevertheless, the cranium of the Mednyi Island fox experienced slightly lower strains during P^4 and M^1 bites compared to the Bering Island fox (Fig. 4, and Supporting Information, Tables S1–S7).

Table 3. Description of landmarks employed in the analysis of deformation

Number	Description
1	The most posterior point on the saggital crest
2	Parietal–frontal suture
3	A point at the internasal suture at the level of maximum concavity of the nasal bones
4	Premaxillary suture at inferior margin of nasal aperture
5	Basion
6	Opisthion
7/8	Posterior root of zygomatic arch, posterior to glenoid
9/10	Lateral point on the postorbital constriction
11/12	Zygomatico-temporal suture on the superior border of the zygomatic arch
13/14	Central zygomatic arch, inferior margin
15/16	Anterior root of zygomatic arch
17/18	Jugal–maxilla dorsal suture, orbital edge
19/20	Infra-orbital foramen, lower margin
21/22	Inferior border of alveolar margin between P^4 and M^1
23/24	Inferior border of alveolar margin between P^3 and P^4
25/26	Premaxilla–maxilla anterior suture at the canine alveola
27/28	Anterior notch of nasal bone
29/30	The most posterior point of palatine fissure
31/32	The most caudal part of the palatine bone
33/34	Protocone of P^4
35/36	Hypocone of M^1
37/38	Auditory bulla, anterior extremity
39/40	Most anterior point on the margin of the tympano-occipital fissure
41/42	Occipital condyle, lateral extremity
43/44	The most ventral point on the auditory bulla
45/46	Meeting point of orbitosphenoid, alisphenoid and frontal sutures
47/48	Most lateral point on the braincase posterior to the postorbital constriction
49/50	Infra-orbital foramen, upper margin

The PCA results of large-scale deformations during simulated biting are presented in Figures 5 and 6, and plots of the first three principal components (PC) are shown. The first PC explained the highest proportion of variance (41.43%), corresponding to the variation in large-scale deformation among bites. The inset warping with overlaid transformation grids indicated that differences along PC1 related mostly to dorsoventral bending of the rostrum. Differences in scores along PC2 (26.84%) are related to differences in the degree of dorsiflexion of the rostrum and in the degree of zygomatic arch deformation among models. Considering PC1 and

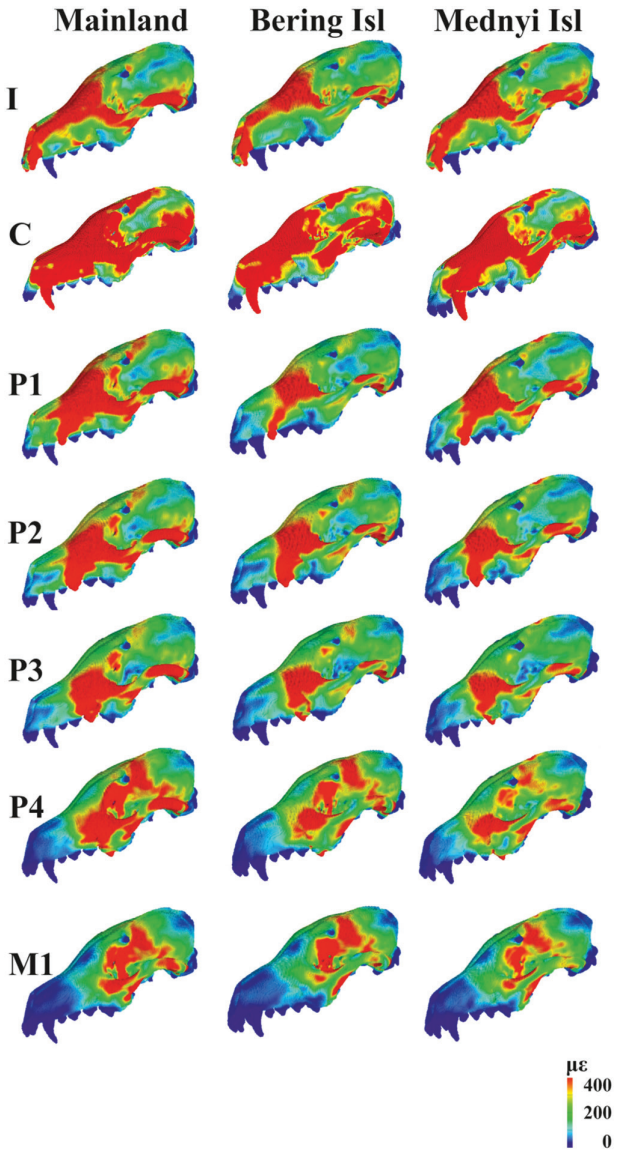

Figure 4. Von Mises strain contour plots of cranial models of the three subspecies of Arctic fox during different simulated 400 N bites. Each row represents a bite on a left tooth: incisors, left I^1, I^2, and I^3 (I); first premolar (P1); second premolar (P2); third premolar (P3); fourth premolar (P4); and first molar (M1). Each column represents a different model. Values are presented as microstrain (με). All strains are scaled to a comparable 400 N bite.

PC2 (Fig. 5), the deformations arising from each bite along the dental row are similar on PC1 and differ on PC2 among the mainland and island Arctic foxes. The inset warping and transformation grids indicate that PC3 (11.35%) distinguishes the unloaded from the loaded crania and relates to torsion of the face during unilateral bites as well as to the degree of rostral dorsiflexion (Fig. 6). The Mednyi Island fox is clearly distinguished from both mainland and Bering Island subspecies along PC3 in showing a smaller degree of deformation (nearer the unloaded).

DISCUSSION

In this study, biomechanical performance was compared among the crania of three Arctic fox subspecies using simulated biting loads. A combination of FE modelling and geometric morphometric methods were employed (O'Higgins *et al.*, 2011; Fitton *et al.*, 2012; O'Higgins & Milne, 2013; Fitton *et al.*, 2015). The results showed differences in local strains and large-scale deformations among subspecies.

The distribution of relative strain magnitudes within the crania was concordant with previous studies in other mammals (Ross, 2001; Wroe *et al.*, 2007; Wroe, 2008; Slater *et al.*, 2009; Slater & Van Valkenburgh, 2009; Fitton *et al.*, 2012; Figueirido *et al.*, 2014), which found that strains in the rostral and frontal region were higher during anterior bites because the bending moment in this region is greater as a consequence of a longer bite force moment arm.

In all bites, the zygomatic arch experienced high strains because of the large muscle mass attached directly to it. Several previous biomechanical studies of mammalian crania that have simulated feeding using FE analyses indicated that the zygomatic arch is a highly stressed area (Dumont *et al.*, 2005, 2011; Bright & Rayfield, 2011; Cox *et al.*, 2012; Fitton *et al.*, 2012). Our findings suggest that the zygomatic arch is not as robust in the mainland subspecies, which likely experiences lower loads from food acquisition and processing. The zygomatic arches bulge more laterally in both the island foxes (Nanova, 2009), possibly to allow a greater cross section and, thus, force production by the temporalis muscle. This may in itself indicate a greater potential for high bite forces. Also, the shape of the arch may be better able to resist high forces, which is concordant with Thomason's (1991) finding that stress mainly correlates with skull shape, but not with size. Slater *et al.* (2009) also noted that among different Carnivora (with different foraging strategies, e.g. *Canis simensis*, *C. mesomelas*, and *Lycaon pictus*), those with more laterally prominent zygomatic arches experience lower strains in this structure, possibly because a more lateral arch is adapted to bear higher loads.

Regarding the PCA of Figure 5, the points representing each loaded cranium within each subspecies are arranged nearly linearly, along PC1. The degree of dorsoventral bending (PC1) declines along the dental row from incisor to molar bites. In Figure 6, PC3 scores reflect cranial torsion (especially in the region of the postorbital constriction; Fig. 6). Smaller degrees of torsion are observed in the Mednyi Island fox for all bites, when

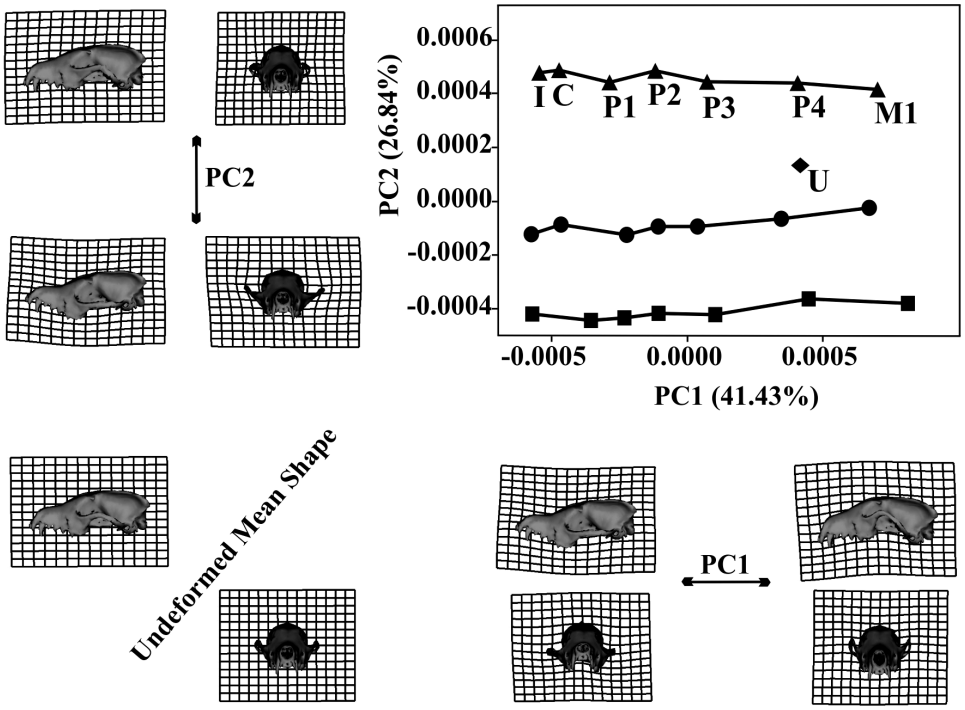

Figure 5. PC plot of size-and-shape coordinates from 50 landmarks representing large-scale cranial deformations during different bites in the three subspecies of Arctic fox. PC1 and PC2 are shown. Triangles, mainland Arctic foxes; circles, Mednyi Island foxes; squares, Bering Island foxes; I (includes I^1, I^2, and I^3), C, P1, P2, P3, P4, and M1 represent the deformations caused by biting on particular teeth. The diamond marked U represents the unloaded undeformed average fox cranium. The aspects of variation in size and shape represented by each PC are visualized as extremes of the PC using transformation grids and the warped surface of the average fox cranium.

compared to the other two subspecies; this may be due its short rostrum (see below). Additionally in all subspecies, less torsion occurs during M^1 simulated bites than during premolar and incisor bites, possibly because of the increased cross-sectional area of the coronal cross section of the cranium in the region immediately above the molar. However, the premolars are anterior to this region, and they are located at the cylindrical part of the rostrum (Ross, 2001; Fitton *et al.*, 2012).

The observed trajectory of deformations was concordant with expectations from the behaviour of simple beams under loading (Greaves, 1985; Thomason 1991; Ross, 2001; Rafferty, Herring & Marshall, 2003; Metzger, Daniel & Ross, 2005; Fitton *et al.*, 2012) in that dorsoventral bending and torsion predominate during anterior and posterior bites, respectively. The deformation of the elongated and narrow rostrum (which has been considered a cylinder or hemi-cylinder; Greaves, 1985) of mainland Arctic foxes was greater than that of the wide rostrum of the Bering Island subspecies or the wide and short rostrum of Mednyi Arctic foxes. These characteristics are similar to the strain pattern that is found in the wide and short rostrum of the African hunting dog (*L. pictus*), which feeds on medium- to large-sized ungulates such as impala, springbok, and kudu in comparison to the long and narrow rostrum of the black-backed jackal (*C. mesomelas*), which feeds generally on small prey such as invertebrates, rodents, hares, and young antelopes (Slater *et al.*, 2009). Strains are generally lower with a short rostrum than with a long and narrow rostrum (Slater *et al.*, 2009). Due its shorter rostrum, the cranium of the Mednyi Island fox is more resistant to torsion in comparison to crania of mainland and Bering Island foxes.

What is the biological significance of these observed differences in cranial biomechanical performance among these subspecies? One possible interpretation is that they represent adaptations related to hunting and feeding habits. For instance, the prey available to Arctic foxes living on the Commander Islands differ from those available to the mainland subspecies (Angerbjörn, Tannerfeldt & Erlinge, 1999; Anthony, Barten & Seiser, 2000; Zagrebelnyi, 2000a; Goltsman *et al.*, 2010), which may impose different adaptive constraints among them. For example, the larger and wider cranium of both island subspecies that results in lower strain and deformation during biting might allow them to resist higher bite loads than the mainland subspecies.

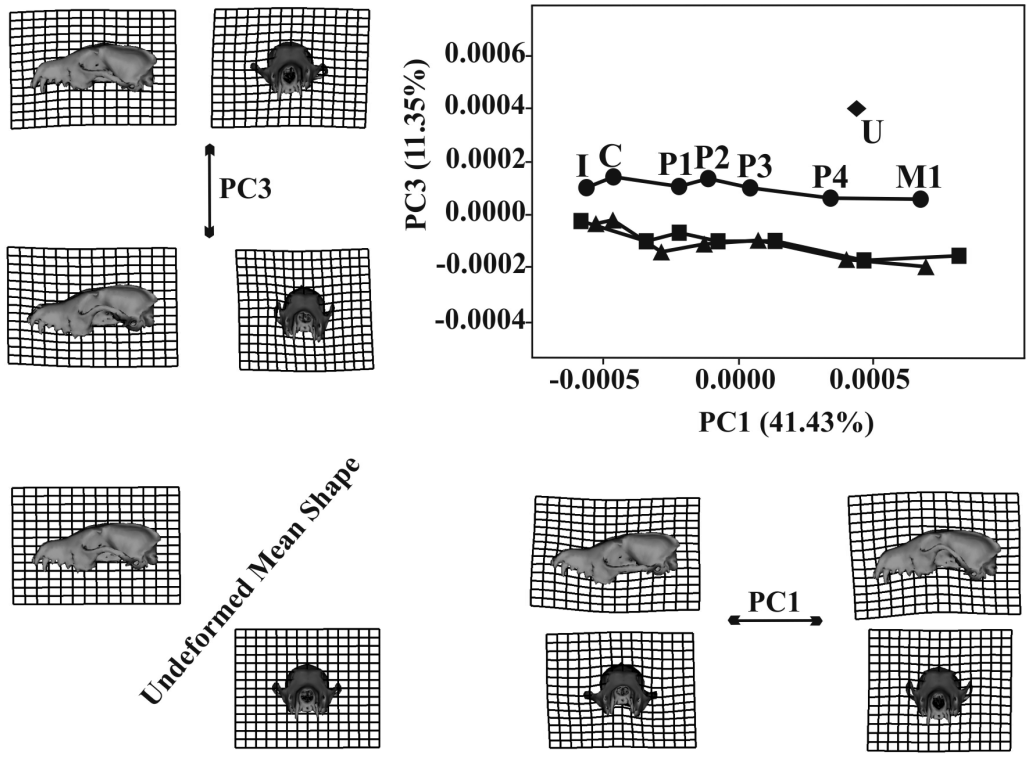

Figure 6. PC plot of size-and-shape coordinates from 50 landmarks representing large-scale cranial deformations during different bites in three subspecies of Arctic fox. PC1 and PC3 are shown. Designations correspond to those in Figure 5.

The diet of island foxes is mainly comprised of seabirds, which are as large as adult foxes, and they often need to be caught and held firmly in the mouth (Sudilovskaya, 1951; Zagrebelnyi, 2000b; Goltsman *et al.*, 2010). In contrast, such birds represent a much smaller proportion of the diet of mainland foxes (Bantle & Alisauskas, 1998), which prey mainly on small rodents that are relatively easy to catch, kill, and consume (Angerbjörn *et al.*, 1999; Anthony *et al.*, 2000; Eide, Jepsen & Prestrud, 2004). Rodents only play a minor role in the diet of the island subspecies (Zagrebelnyi, 2000b).

These findings on cranial biomechanical performance of these same subspecies are concordant with results on cranial morphology and gape (Nanova & Prôa, 2017). An enlarged gape angle in both island populations was found, which is necessary when foraging on large prey. Moreover, a rostrum contraction was found in the Mednyi Island Arctic foxes (Nanova & Prôa, 2017) which provides further evidence for cranial resistance to deformation during biting at larger gape. Thus, plausibly, the larger and more robust crania of the two island foxes reflect greater ability to resist extrinsic loads.

In conclusion, the two island subspecies and the mainland subspecies of Arctic fox showed phenotypic differences in cranial form, local strains, and large-scale deformations of the cranium during biting simulations. These may mirror adaptations to different diets that set the mainland subspecies apart from the island subspecies, but it is not possible to say with certainty that these differences are indeed adaptive. Furthermore, the two studied island foxes were isolated during the same time period in similar environmental conditions, but they differ slightly in cranial morphology and biomechanics (compared to differences between island and mainland foxes). However, these differences cannot be interpreted as adaptive divergence. Although island and mainland foxes hunt and consume different prey, the biomechanical requirements necessary to capture and break down each type of prey are not presently known. More data associated with food acquisition and the physical properties of each prey type are required to assess the extent to which the present findings reflect biomechanical adaptations to diet and prey acquisition.

ACKNOWLEDGEMENTS

We wish to thank V.S. Lebedev, M.E. Goltsman, A.N. Shienok, and V. Toro-Ibacache for discussing different

parts of this work. We also thank four reviewers whose comments considerably improved this paper. This study was supported by a Royal Society International Joint Project 100455, a grant from the President of Russian Federation MK- MK-1681.2012.4, and a grant RFBR 12-04-31013 mol_a, and RSCF grant 14-50-00029 from which Editage service was paid. MP was funded by the Fundação para a Ciência e a Tecnologia (doctoral fellowship SFRH/BD/33852/2009), through the PhD Programme in Computational Biology, Instituto Gulbenkian de Ciência, Portugal. The authors declare no conflict of interest.

REFERENCES

Andersson K, Norman D, Werdelin L. 2011. Sabretoothed carnivores and the killing of large prey. *PLoS One* **6:** e24971.

Angerbjörn A, Tannerfeldt M, Erlinge S. 1999. Predator-prey relationships: arctic foxes and lemmings. *Journal of Animal Ecology* **68:** 34–49.

Anthony RM, Barten NL, Seiser PE. 2000. Foods of arctic foxes (*Alopex lagopus*) during winter and spring in western Alaska. *Journal of Mammalogy* **81:** 820–828.

Antón SC. 1999. Macaque masseter muscle: internal architecture, fiber length and cross-sectional area. *International Journal of Primatology* **20:** 441–462.

Bannikov AG. 1970. Arctic fox in the U.S.S.R.: biological premises of productivity. In: Fuller WA, Kevan PG, eds. *Productivity and conservation in northern circumpolar land.* Morges: IUCN, 121–129.

Bantle JL, Alisauskas RT. 1998. Spatial and temporal patterns in arctic fox diets at a large goose colony. *Arctic* **51:** 231–236.

Barabash-Nikiforov II. 1937. On the biology of Commander Island arctic foxes [in Russian]. *Proceedings of Arctic Institute* **65:** 145–167.

Barabash-Nikiforov II. 1939. On the diet of Mednyi Island arctic foxes *Alopex beringensis semenovi* Ogn [in Russian]. *Bulletin of Moscow Society of Naturalists* **48:** 74–80.

Bookstein FL. 2013. Allometry for the twenty-first century. *Biol. Theory* **7:** 10–25.

Braestrup FW. 1941. A study of the Arctic Fox in Greenland. Immigrations fluctuations in numbers based mainly on trading statistics. *Meddelelser om Gronland* **131:** 1–10.

Bright JA, Rayfield EJ. 2011. Sensitivity and ex vivo validation of finite element models of the domestic pig cranium. *Journal of Anatomy* **219:** 456–471.

Chelnokov FG. 1970. On the relationship between foxes and fur-seal cubs [in Russian]. *Problems of Kamchatka Geography* **6:** 151–158.

Christiansen P. 2007. Evolutionary implications of bite mechanics and feeding ecology in bears. *Journal of Zoology* **272:** 423–443.

Christiansen P, Adolfssen JS. 2005. Bite forces, canine strength and skull allometry in carnivores (Mammalia, Carnivora). *Journal of Zoology* **266:** 133–151.

Christiansen P, Wroe S. 2007. Bite forces and evolutionary adaptations to feeding ecology in carnivores. *Ecology* **88:** 347–358.

Cox PG, Fagan MJ, Rayfield EJ, Jeffery N. 2011. Finite element modelling of squirrel, guinea pig and rat skulls: using geometric morphometrics to assess sensitivity. *Journal of Anatomy* **219:** 696–709.

Cox PG, Rayfield EJ, Fagan MJ, Herrel A, Pataky TC, Jeffery N. 2012. Functional evolution of the feeding system in rodents. *PLoS One* **7:** e36299.

Dalén L, Fuglei E, Hersteinsson P, Kapel CMO, Roth JD, Samelius G, Tannerfeldt M, Angerbjörn A. 2005. Population history and genetic structure of a circumpolar species: the arctic fox. *Biological Journal of the Linnean Society* **84:** 79–89.

Dalerum F., Angerbjörn A. 2000. Arctic fox (*Alopex lagopus*) diet in Karupelv valley, East Greenland, during a summer with low lemming density. *Arctic* **53:** 1–8.

Demes B, Creel N. 1988. Bite force, diet, and cranial morphology of fossil hominids. *Journal of Human Evolution* **17:** 657–670.

Dumont ER, Davis JL, Grosse IR, Burrows AM. 2011. Finite element analysis of performance in the skulls of marmosets and tamarins. *Journal of Anatomy* **218:** 151–162.

Dumont ER, Piccirillo J, Grosse IR. 2005. Finite-element analysis of biting behavior and bone stress in the facial skeletons of bats. *The Anatomical Record. Part A* **283:** 319–330.

Dzhykiya EL. 2008. *Genetic polymorphism of Commander Islands' Arctic Foxes (Alopex lagopus semenovi, Ognev 1931, Alopex lagopus beringensis, Merriam 1902) [in Russian].* Unpublished D.Phil. Thesis, Moscow State University of M.V. Lomonosov.

Eide NE, Jepsen JU, Prestrud P. 2004. Spatial organization of reproductive Arctic foxes *Alopex lagopus*: responses to changes in spatial and temporal availability of prey. *Journal of Animal Ecology* **73:** 1056–1068.

Ellis JL, Thomason JJ, Kebreab E, France J. 2008. Calibration of estimated biting forces in domestic canids: comparison of post-mortem and in vivo measurements. *Journal of Anatomy* **212:** 769–780.

Fagan MJ, Curtis N, Dobson CA, Kupczik K, Moazen M, Page L, Phillips R, O'Higgins P. 2007. Voxel-based finite element analysis—working directly with microCT scan data. *Journal of Morphology* **268:** 1071–1071.

Figueirido B, Palmqvist P, Pérez-Claros JA. 2009. Ecomorphological correlates of craniodental variation in bears and paleobiological implications for extinct taxa: an approach based on geometric morphometrics. *Journal of Zoology* **277:** 70–80.

Figueirido B, Palmqvist P, Pérez-Claros JA, Dong W. 2011. Cranial shape transformation in the evolution of the giant panda (*Ailuropoda melanoleuca*). *Die Naturwissenschaften* **98:** 107–116.

Figueirido B, Tseng ZJ, Serrano-Alarcón FJ, Martín-Serra A, Pastor JF. 2014. Three-dimensional computer simulations of feeding behaviour in red and giant pandas relate skull biomechanics with dietary niche partitioning. *Biology Letters* **10:** 20140196.

Fitton LC. 2007. *Form-function complex of the primate masticatory apparatus. An investigation into the form-function complex of the Cercopithecinae masticatory apparatus using computer modelling*. Unpublished Ph.D. Thesis, University of Liverpool.

Fitton LC, Prôa M, Rowland C, Toro-Ibacache V, O'higgins P. 2015. The impact of simplifications on the performance of a finite element model of a *Macaca fascicularis* cranium. *Anatomical Record* **298:** 107–121.

Fitton LC, Shi JF, Fagan MJ, O'Higgins P. 2012. Masticatory loadings and cranial deformation in *Macaca fascicularis*: a finite element analysis sensitivity study. *Journal of Anatomy* **221:** 55–68.

Geffen E, Waidyaratne S, Dalén L, Angerbjörn A, Vila C, Hersteinsson P, Fuglei E, White PA, Goltsman M, Kapel CM, *et al*. 2007. Sea ice occurrence predicts genetic isolation in the Arctic fox. *Molecular Ecology* **16:** 4241–4255.

Goltsman M, Kruchenkova EP, Macdonald DW. 1996. The Mednyi arctic foxes: treating a population imperilled by disease. *Oryx* **30:** 251–258.

Goltsman M, Kruchenkova EP, Sergeev S, Volodin I, Macdonald DW. 2005. "Island syndrome" in a population of Arctic foxes (*Alopex lagopus*) from Mednyi Island. *Journal of Zoology* **267:** 405–418.

Goltsman ME, Nanova OG, Sergeev SN, Shienok AN. 2010. Food habits of the arctic fox (*Alopex lagopus semenovi*) on Mednyi island (North Pacific, Commander Islands) [in Russian]. *Zoologicheskii Zhurnal* **89:** 1246–1263.

Gould SJ, Eldredge N. 1977. Punctuated equilibria: the tempo and mode of evolution reconsidered. *Paleobiology* **3:** 115–151.

Greaves WS. 1985. The mammalian postorbital bar as a torsion-resisting helical strut. *Journal of Zoology* **207:** 125–136.

Gröning F, Fagan MJ, O'Higgins P. 2011. The effects of the periodontal ligament on mandibular stiffness: a study combining finite element analysis and geometric morphometrics. *Journal of Biomechanics* **44:** 1304–1312.

Hammer Ø, Harper DAT, Ryan PD. 2001. Past: paleontological statistics software package for education and data analysis. *Palaeontologia Electronica* **4:** art. 4.

Herring SW, Herring SE. 1974. The superficial masseter and gape in mammals. *The American Naturalist* **108:** 561–576.

Huskey SH, Turingan RG. 2001. Variation in prey-resource utilization and oral jaw gape between two populations of Largemouth Bass, *Micropterus salmoides*. *Environmental Biology of Fishes* **61:** 185–194.

Ilyina ED. 1950. *Fur Farming on Islands [in Russian]*. Moscow: Mezhdunarodnaya Kniga.

Kupczik K, Dobson CA, Fagan MJ, Crompton RH, Oxnard CE, O'Higgins P. 2007. Assessing mechanical function of the zygomatic region in macaques: validation and sensitivity testing of finite element models. *Journal of Anatomy* **210:** 41–53.

Kupczik K, Stynder DD. 2012. Tooth root morphology as an indicator for dietary specialization in carnivores (Mammalia: Carnivora). *Biological Journal of the Linnean Society* **105:** 456–471.

Lindauer SJ, Gay T, Rendell J. 1993. Effect of jaw opening on masticatory muscle EMG-force characteristics. *Journal of Dental Research* **72:** 51–55.

Liu J, Shi J, Fitton LC, Phillips R, O'Higgins P, Fagan MJ. 2012. The application of muscle wrapping to voxel-based finite element models of skeletal structures. *Biomechanics and Modeling in Mechanobiology* **11:** 35–47.

Marakov SV. 1964. *Mammals and birds of Commander Islands [in Russian]*. Unpublished Ph.D. Thesis, Research Institute of Hunting and Fur Farming, Kirov.

Mayr E. 1967. The challenge of island faunas. *Australian Natural History* **15:** 369–374.

McHenry CR, Clausen PD, Daniel WJ, Meers MB, Pendharkar A. 2006. Biomechanics of the rostrum in crocodilians: a comparative analysis using finite-element modeling. *The Anatomical Record. Part A* **288:** 827–849.

Metzger KA, Daniel WJ, Ross CF. 2005. Comparison of beam theory and finite-element analysis with in vivo bone strain data from the alligator cranium. *The Anatomical Record. Part A* **283:** 331–348.

Millien V. 2006. Morphological evolution is accelerated among island mammals. *PLoS Biology* **4:** e321.

Nanova OG. 2009. *Structure of morphological disparity in three species of extant Carnivora (Mammalia: Carnivora) [in Russian]*. Unpublished Doctoral Thesis, Moscow State University.

Nanova OG. 2010. Age variability of morphometrics features in skulls of the mainland arctic fox (*Alopex lagopus lagopus*) and the Commander arctic fox (*A. l. beringensis*, *A. l. semenovi*) [in Russian]. *Zoologicheskii Zhurnal* **89:** 871–881.

Nanova OG, Prôa M. 2017. Cranial features of mainland and Commander Islands Arctic foxes *Vulpes lagopus* reflect their diverging foraging strategies. *Polar Research*. In Press.

Naumov NP, Goltsman ME, Kruchenkova EP, Ovsynnikov NG, Popov SV, Smirin VM. 1981. Social behaviour of arctic foxes on Mednyi Island. Factors determining the spatial-temporal mode of activity [in Russian]. In: Kuznecov GV, Naumov NP, eds. *Ecology, population structure, intraspecific communication processes in mammals*. Moscow: Nauka, 31–75.

O'Higgins P, Cobb SN, Fitton LC, Gröning F, Phillips R, Liu J, Fagan MJ. 2011. Combining geometric morphometrics and functional simulation: an emerging toolkit for virtual functional analyses. *Journal of Anatomy* **218:** 3–15.

O'Higgins P, Milne N. 2013. Applying geometric morphometrics to compare changes in size and shape arising from finite elements analyses. *Hystrix, the Italian Journal of Mammalogy* **24:** 7.

Parr WC, Wroe S, Chamoli U, Richards HS, McCurry MR, Clausen PD, McHenry C. 2012. Toward integration of geometric morphometrics and computational biomechanics: new methods for 3D virtual reconstruction and quantitative analysis of finite element models. *Journal of Theoretical Biology* **301:** 1–14.

Rafferty KL, Herring SW, Marshall CD. 2003. Biomechanics of the rostrum and the role of facial sutures. *Journal of Morphology* **257:** 33–44.

van Rietbergen B, Weinans H, Huiskes R, Polman BJW. 1996. Computational strategies for iterative solutions of large FEM applications employing voxel data. *International Journal for Numerical Methods in Engineering* **39:** 2743–2767.

Ross CF. 2001. In vivo function of the craniofacial haft: the interorbital "pillar". *American Journal of Physical Anthropology* **116:** 108–139.

Sacco T, Van Valkenburgh B. 2004. Ecomorphological indicators of feeding behaviour in the bears (Carnivora: Ursidae). *Journal of Zoology* **263:** 41–54.

Slater GJ, Dumont ER, Van Valkenburgh B. 2009. Implications of predatory specialization for cranial form and function in canids. *Journal of Zoology* **278:** 181–188.

Slater GJ, Figueirido B, Louis L, Yang P, Van Valkenburgh B. 2010. Biomechanical consequences of rapid evolution in the polar bear lineage. *PLoS One* **5:** e13870.

Slater GJ, Van Valkenburgh B. 2009. Allometry and performance: the evolution of skull form and function in felids. *Journal of Evolutionary Biology* **22:** 2278–2287.

Smirin VM, Goltsman ME, Kruchenkova EP, Ovsynnikov NG, Safronov OV. 1979. Behaviour of arctic foxes on the fur-seals rookery [in Russian]. In: Sokolov VE, ed. *Ecologycal foundations of conservation and management of carnivores mammals*. Moscow: Nauka, 164–165.

Sokolov VE. 1979. *Systematics of mammals. V3 [in Russian].* Moscow: High school press.

Sudilovskaya AM. 1951. Procellariiformes (or tubenoses) [in Russian]. In: Dementiev GP, Gladkov NA, eds. *Birds of USSR, V2*. Moscow: Nauka, 287–340.

Tcalkin VI. 1944. Cranium geographic variation of Eurasian arctic foxes [in Russian]. *Zoologicheskii Zhurnal* **23:** 156–169.

Thomason JJ. 1991. Cranial strength in relation to estimated biting forces in some mammals. *Canadian Journal of Zoology* **69:** 2326–2333.

Verrue V, Dermaut L, Verhegghe B. 2001. Three-dimensional finite element modelling of a dog skull for the simulation of initial orthopaedic displacements. *European Journal of Orthodontics* **23:** 517–527.

Weijs WA, Hillen B. 1985. Physiological cross-section of the human jaw muscles. *Acta Anatomica* **121:** 31–35.

Wroe S. 2008. Cranial mechanics compared in extinct marsupial and extant African lions using a finite-element approach. *Journal of Zoology* **274:** 332–339.

Wroe S. 2010. Cranial mechanics of mammalian carnivores: recente advances using a finite element approach. In: Goswami A, Friscia A, eds. *Carnivoran evolution: new views on phylogeny, form, and function*. Cambridge: Cambridge University Press, 466–485.

Wroe S, Clausen P, McHenry C, Moreno K, Cunningham E. 2007. Computer simulation of feeding behaviour in the thylacine and dingo as a novel test for convergence and niche overlap. *Proceedings of the Royal Society B Biological Sciences* **274:** 2819–2828.

Zagrebelnyi SV. 2000a. Feeding ecology of Commander Islands arctic fox subspecies: from Bering Island (*Alopex lagopus beringensis* Merriam 1902) and Mednyi Island (*A.l. semenovi* Ognev 1931; Carnivora, Canidae) [in Russian]. *Zoologicheskii Zhurnal* **79:** 595–697.

Zagrebelnyi SV. 2000b. *Commander Islands Arctic Fox Subspecies (Alopex lagopus beringensis Merriam, 1902 and Alopex lagopus semenovi Ognev, 1931): features of island populations [in Russian].* Unpublished Doctoral Thesis, Commander Islands Natural Reserve and Moscow State University.

Zagrebelnyi SV, Puzachenko AY. 2006. Craniological variability of arctic foxes of Bering Island *Alopex lagopus beringensis*, Mednyi Island *A.l. semenovi*, and mainland *A.l. lagopus* subspecies (Carnivora, Canidae) [in Russian]. *Zoologicheskii Zhurnal* **85:** 1007–1023.

SUPPORTING INFORMATION

Additional Supporting Information may be found in the online version of this article at the publisher's website:

Table S1. Strain magnitudes from FEAs of simulated incisor biting in the three models. Maximum (ε1) and minimum (ε3) principal strain magnitudes at the 50 landmark locations are displayed in microstrain (με). Also displayed strain differences (Δε1 and Δε3) between models at the landmark locations.

Table S2. Strain magnitudes from FEAs of simulated canine biting in the three models. Maximum (ε1) and minimum (ε3) principal strain magnitudes at the 50 landmark locations are displayed in microstrain (με). Also displayed strain differences (Δε1 and Δε3) between models at the landmark locations.

Table S3. Strain magnitudes from FEAs of simulated biting on the first upper premolar in the three models. Maximum (ε1) and minimum (ε3) principal strain magnitudes t at the 50 landmark locations are displayed in microstrain (με). Also displayed strain differences (Δε1 and Δε3) between models at the landmark locations.

Table S4. Strain magnitudes from FEAs of simulated biting on the second upper premolar in the three models. Maximum (ε1) and minimum (ε3) principal strain magnitudes t at the 50 landmark locations are displayed in microstrain (με). Also displayed strain differences (Δε1 and Δε3) between models at the landmark locations.

Table S5. Strain magnitudes from FEAs of simulated biting on the third upper premolar in the three models. Maximum (ε1) and minimum (ε3) principal strain magnitudes t at the 50 landmark locations are displayed in microstrain (με). Also displayed strain differences (Δε1 and Δε3) between models at the landmark locations.

Table S6. Strain magnitudes from FEAs of simulated biting on the fourth upper premolar in the three models. Maximum (ε1) and minimum (ε3) principal strain magnitudes t at the 50 landmark locations are displayed in microstrain (με). Also displayed strain differences (Δε1 and Δε3) between models at the landmark locations.

Table S7. Strain magnitudes from FEAs of simulated biting on the first upper molar in the three models. Maximum (ε1) and minimum (ε3) principal strain magnitudes t at the 50 landmark locations are displayed in microstrain (με). Also displayed strain differences (Δε1 and Δε3) between models at the landmark locations.